Nanoscale

PAPER

View Article Online
View Journal | View Issue

Cite this: *Nanoscale*, 2016, **8**, 19592

Strong *in vivo* antitumor responses induced by an antigen immobilized in nanogels *via* reducible bonds†

Dandan Li,[a] Feilong Sun,[a] Meriem Bourajjaj,[a] Yinan Chen,[a] Ebel H. Pieters,[a] Jian Chen,[a] Joep B. van den Dikkenberg,[a] Bo Lou,[a] Marcel G. M. Camps,[b] Ferry Ossendorp,[b] Wim E. Hennink,[a] Tina Vermonden[a] and Cornelus F. van Nostrum*[a]

Received 14th July 2016,
Accepted 26th September 2016

DOI: 10.1039/c6nr05583d

www.rsc.org/nanoscale

Cancer vaccines are at present mostly based on tumor associated protein antigens but fail to elicit strong cell-mediated immunity in their free form. For protein-based vaccines, the main challenges to overcome are the delivery of sufficient proteins into the cytosol of dendritic cells (DCs) and processing by, and presentation through, the MHC class I pathway. Recently, we developed a cationic dextran nanogel in which a model antigen (ovalbumin, OVA) is reversibly conjugated *via* disulfide bonds to the nanogel network to enable redox-sensitive intracellular release. In the present study, it is demonstrated that these nanogels, with the bound OVA, were efficiently internalized by DCs and were capable of maturating them. On the other hand, when the antigen was just physically entrapped in the nanogels, OVA was prematurely released before the particles were taken up by cells. When combined with an adjuvant (polyinosinic–polycytidylic acid, poly(I:C)), nanogels with conjugated OVA induced a strong protective and curative effect against melanoma *in vivo*. In a prophylactic vaccination setting, 90% of the mice vaccinated with nanogels with conjugated OVA + poly(I:C) did not develop a tumor. Moreover, in a therapeutic model, 40% of the mice showed clearance of established tumors and survived for the duration of the experiment (80 days) while the remaining mice showed substantial delay in tumor progression. In conclusion, our results demonstrate that conjugation of antigens to nanogels *via* reducible covalent bonds for intracellular delivery is a promising strategy to induce effective antigen-specific immune responses against cancer.

1. Introduction

With the increasing interest in immunotherapy as a potential strategy against cancers, specific subunits, such as protein antigens, are being used to develop safe and well-defined vaccines.[1–3] Moreover, these subunits are suited for GMP production. However, because of their poor immunogenicity, these protein antigens on their own often evoke weak and short-lived humoral and cellular immune responses, and in particular, fail to elicit a $CD8^+$ cytotoxic T cell response.[4–7] Currently, there is still a lack of efficacious vaccines against many types of cancer and infections that require both humoral and cellular immunity for the required therapeutic effects. Soluble protein antigens are endocytosed by APCs (antigen presenting cells) and subsequently degraded into antigenic peptides in endo/lysosomal compartments.[4–7] Those antigenic peptides in lysosomes can be presented by MHC (major histocompatibility complex) class II molecules to $CD4^+$ T-helper cells, which can induce both cellular and humoral immunity *i.e.* helping B cells to produce antibodies.[4] However, for effective vaccination against cancer, it is crucial that APCs present antigenic peptides through the MHC class I pathway to $CD8^+$ cytotoxic T cells (CTLs), and these activated CTLs in turn attack tumor cells that express the same antigenic peptide determinants.[8,9] The key challenges for optimal vaccine design are to deliver antigens to the correct APCs, which are known as dendritic cells (DCs),[9–11] and to transport antigenic peptides to the cytosol of DCs, resulting in subsequent presentation in MHC class II and class I pathways (so-called cross-presentation).[12–14]

Recent efforts to make effective and safe vaccines against cancer have focused on developing particulate delivery systems for antigens to induce robust CTL responses. Among the

[a]*Department of Pharmaceutics, Utrecht Institute for Pharmaceutical Sciences, Utrecht University, Utrecht 3584CG, The Netherlands. E-mail: C.F.vanNostrum@uu.nl*
[b]*Department of Immunohematology and Blood Transfusion, Leiden University Medical Center, Leiden 2333ZA, The Netherlands*

†Electronic supplementary information (ESI) available. See DOI: 10.1039/c6nr05583d

nano/microparticulate vaccines, they all showed that the immune efficacy of the loaded antigen increased to a greater or lesser extent.[15–25] To achieve effective vaccination, the first step is to ensure that the antigen remains associated with the carrier and that sufficient antigen loaded particles are taken up by DCs. After internalization, the second required step is the release and processing of the loaded antigen. Particulate carriers are usually internalized by APCs and end up in compartments such as endo/lysosomes in which the antigens are mostly degraded and subsequently enter the MHC class II antigen presentation pathway. To enable MHC class I antigen presentation, some delivery systems have been designed to escape from endosomes (pH-responsive polymeric particles and particles modified with fusion peptides) to facilitate antigen cross-presentation.[26–28] In addition, some carriers, such as virus-like particles and cationic particles, display excellent adjuvant properties.[29–32] They provide sufficient danger signals to alert DCs and are capable of inducing both innate and cognate immune responses.

In our previous study,[33] we designed and synthesized reduction-sensitive cationic dextran nanogels to control antigen release after their uptake by APCs. A protein antigen (ovalbumin, OVA) was reversibly immobilized in the nanogels *via* disulfide bonds with relatively high loading capacity. An important advantage of this system is that the antigen remained stably entrapped in a non-reducing environment, whereas triggered release occurred in reductive environments. These nanogels showed intracellular release of the antigen in DCs and boost MHC class I antigen presentation. In the present paper, we will show the results of the influence of nanogel size and surface charge on the uptake by DCs, the capability of the nanogels to maturate DCs, the intracellular delivery, transportation and processing of antigen by DCs *in vitro*, and therapeutic and prophylactic vaccination with nanogels with conjugated antigen *in vivo*.

2. Experimental section

2.1 Materials

Egg albumin (OVA) was obtained from Worthington (USA). Trimethyl aminoethyl methacrylate 80% aqueous solution (TMAEMA), 2-aminoethyl methacrylate hydrochloride, ethylenediamine tetraacetic acid (EDTA) and hydroxylamine were purchased from Sigma Aldrich. Methacrylated dextran (dex-MA, M_w 40 000 Da, degree of methacrylate substitution = 8) and *N*-(4-(2-(pyridine-2-yldisulfanyl)ethyl)-amidobutyl)methacrylamide were synthesized as previously reported.[33–35] All the fluorescent dyes and markers were provided by Invitrogen.

2.2 Cell line, cell culture, and animals

The D1 cell line,[36] a long-term growth factor-dependent immature myeloid dendritic cell line of splenic origin derived from a female C57BL/6 mouse, was cultured in IMDM (Iscove's Modified Dulbecco's Medium, Lonza) containing 10% heat-inactivated FBS (Sigma), 2 mM GlutaMax (GIBCO), 50 μM β-mercaptoethanol and 30% supernatant from R1 cells (mouse fibroblast NIH/3T3 cells transfected with mouse GM-CSF gene), which was collected from confluent cultures and filtered. The B16-OVA cell line,[37] a stable OVA-transfectant derived from the murine melanoma cell line B16, was maintained in RPMI 1640 medium (Sigma) supplemented with 10% fetal bovine serum (Sigma) and 1 mg mL^{-1} of G418 (Sigma). Inbred, 5–7-week old female C57BL/6 mice were obtained from Charles River Laboratories (Maastricht, Netherlands). All mice were housed at the Laboratory Animal Facility of the Utrecht University and treated according to the regulations of the animal ethics committee of the Netherlands. All experiments were approved by the animal experimental committee of Utrecht University, the Netherlands.

2.3 Preparation and characterization of OVA-loaded nanogels

Cationic dextran nanogels were prepared by inverse mini-emulsion photo-polymerization of methacrylated dextran (120 mg), trimethyl aminoethyl methacrylate (160 μL) and a pyridyldisulfide-containing methacrylamide monomer, *N*-(4-(2-(pyridine-2-yldisulfanyl)ethyl)-amidobutyl)methacrylamide (5 mg), as previously reported.[33] To label the particles, amino groups were introduced by preparing them in the presence of 2 mol% (of dextran and TMAEMA) 2-aminoethyl methacrylate hydrochloride.[38] The latter particles (20 mg) were incubated with Alexa 488 dye (Alexa Fluor 488 NHS Ester (succinimidyl ester), 1 mg ml^{-1}, 15 μL) in sodium bicarbonate solution (100 mM, pH 8.4) for 2 h. Subsequently, the particles were washed with water and spun down until no free dye was found in the supernatant (determined by FLUOstar OPTIMA (BMG LABTECH), and the washing was repeated 3 times). OVA solution (native or derivatized with SATA (on the average 2.7 modifications on one OVA molecule as previously reported),[33] 2 mg mL^{-1}, 7.5 mL) was mixed with nanogel suspension (2 mg mL^{-1}, 42.5 mL) in HEPES buffer (20 mM, pH 7.4). The mixture was incubated at room temperature for 1 h to allow OVA loading into the particles. Subsequently, a deacetylation solution (1.72 g hydroxylamine 50% aqueous solution, 0.365 g EDTA in 50 mL HEPES buffer (20 mM, pH 7.4), 5 mL) was added and the mixture was incubated for 2 h at room temperature. The OVA loaded particles were collected and purified by multiple washing (with 20 mM HEPES for native OVA or PBS for SATA-derivatized OVA) and centrifugation steps, and then lyophilized. The sizes and zeta-potentials of the nanogels were measured in HEPES (20 mM) using DLS (Malvern ALV/CGS-3 Goniometer, Malvern Instruments, Malvern, UK) and Zetasizer (Zetasizer Nano, Malvern Instruments, USA), respectively. The loading capacity was determined by measuring the OVA concentration in the washing fluids with a UPLC system (Waters, USA) as described.[33]

2.4 Interaction between OVA loaded particles and DCs

Nanogels loaded with native or SATA-modified DQ-OVA (OVA labeled with BODIPY (boron-dipyrromethene) dyes, Invitrogen) were prepared as described above. D1 cells (70 000 cells in 200 μL medium per well) were incubated with the DQ-OVA

Table 1 Characterization (*Z*-average hydrodynamic diameter (Z_{ave}), polydispersity index (PDI), zeta potential, and loading capacity) of dextran particles dispersed in HEPES buffer (20 mM, pH 7.4). Mean values with corresponding standard deviations are shown (n = 3)

Dextran particles	Z_{ave} (nm)	PDI	Size (μm) ± SD	ζ-Potential (mV)	Loading capacity (wt%)
Nanogels with conjugated OVA	207 ± 3	0.07 ± 0.01		20.6 ± 0.7	11.7 ± 0.1
Nanogels with native OVA	198 ± 6	0.13 ± 0.02		20.6 ± 0.3	11.1 ± 0.1
Nanogels (low charge) with conjugated OVA	225 ± 7	0.12 ± 0.04		12.2 ± 0.6	10.5 ± 0.3
Nanogels (neutral)	213 ± 8	0.17 ± 0.03		−0.2 ± 0.1	—
Microgels with conjugated OVA			2.5 ± 1.4	22.3 ± 0.2	14.3 ± 0.2

loaded nanoparticles (final concentration of nanogel-associated OVA was 2.5 μg mL^{-1}), or with Alexa-labeled dextran particles (as shown in Table 1, having a final concentration of 25 μg mL^{-1}) for various times (2, 5, or 24 h at 37 or at 4 °C). The viability of D1 cells incubated with these dextran particles was reported previously and no cytotoxicity was observed at the particle concentration used in this study.[33] Subsequently, images were taken by confocal laser scanning microscopy (CLSM, Confocal Leica SPE-II, Leica Microsystems) before and after quenching with trypan blue (1 mg mL^{-1}, 30 μL per dish, confocal images were taken within 30 min after addition of trypan blue to cells).[39] For lysosome staining, lysotracker-red was added 1 h before imaging.

For quantification of the uptake, the D1 cells were detached (with 2 mM EDTA PBS buffer) after incubation with particles for 24 h, and their fluorescence intensity with or without quenching with trypan blue was detected using flow cytometry (BD FACSCANTO II, BD Biosciences). To measure the maturation level of the D1 cells after incubation with different particles for 24 h, the cells were washed with FACS buffer and subsequently stained with anti-CD40-FITC and anti-CD86-PE antibodies (2 μg mL^{-1}, 25 μL per well, eBioscience) for 30 min on ice. These D1 cells were subsequently analyzed by flow cytometry after being washed with FACS buffer. The cell culture supernatant was diluted (from 250 up to 32 000 times) for analysis for interleukin 12 (IL-12 p40) with a cytokine-specific ELISA kit (NOVEX).[40]

2.5 Prophylactic vaccination

For the prophylactic treatment study, 8 groups of mice (n = 10) were immunized twice (prime and boost) at an interval of 2 weeks s.c. in the left flank with different vaccine formulations comprising 50 μg of OVA (and 20 μg of poly(I:C)) in 100 μL PBS. These 8 groups included mice treated with (1) PBS only, (2) empty cationic nanogels, (3) native OVA, (4) native OVA + poly(I:C), (5) nanogels with native OVA, (6) nanogels with native OVA + poly(I:C), (7) nanogels with conjugated OVA, and (8) nanogels with conjugated OVA + poly(I:C). Two weeks after the last vaccination, 1.5×10^5 OVA-expressing melanoma cells (B16-OVA) suspended in 100 μL PBS were inoculated s.c. on the opposite flank.[41,42] The tumor size was measured every other day using a caliper in two vertical dimensions, and tumor size in mm^3 was calculated by length × $width^2/2$. Mice were euthanized when the volume reached 2000 mm^3 according to ethical guidelines. One week after the prime and boost vaccination, blood samples were collected *via* submandibular bleeding in heparinized tubes for detecting OVA specific $CD8^+$ cells and in Eppendorf tubes for measuring the OVA-specific antibody.[17,37,43]

2.6 Therapeutic vaccination

For therapeutic immunization, 1.5×10^5 B16-OVA tumor cells (in 100 μL PBS) were first injected s.c. into the mouse right flank.[44,45] Tumors were monitored every other day for tumor onset and upon the appearance of palpable tumors (~2 × 2 mm, around day 6), the various formulations were injected s.c. on the opposite flank (groups and doses are as mentioned in prophylactic vaccination). Ten days after the prime, the mice within each group received boost injections with the same formulation as the prime. The tumor size of each mouse was measured every other day and tumor volumes were calculated as described above. Mice were sacrificed when humane end-points (tumor volume >2000 mm^3) were met. One week after the prime and boost vaccination, blood was taken *via* submandibular bleeding for measuring OVA specific $CD8^+$ cells and the OVA-specific antibody.

2.7 Tetramer staining

Blood samples collected *via* submandibular bleeding in heparinized tubes were analyzed for OVA specific $CD8^+$ T cells.[44,45] Red blood cells were lysed by red blood cell lysis buffer (Roche) and the remaining cells (mainly leukocytes) were washed with 2% BSA in PBS (FACS buffer) and spun down. T cells then were stained with APC-conjugated SIINFEKL/H2-Kb tetramers (Leiden University Medical Center, the Netherlands) and PE-conjugated anti-mouse CD8a mAb (BD Bioscience) for 1 h on ice. After tetramer staining, cells were washed with FACS buffer and suspended in 100 μL of FACS buffer. Data were acquired using flow cytometry. The gating strategy for analysis of % H-2Kb OVA tetramer $CD8^+$ T cells is described in ESI Fig. S2.†

2.8 Determination of anti-OVA antibody titers in serum

For the detection of anti-OVA antibody titers in immunized mice, serum was separated from clotted blood after overnight storage at 4 °C and subsequent centrifugation (2000*g*, 10 min). The titers of OVA specific antibodies in the different serum samples of the mice were quantitatively determined by ELISA. Briefly, microtiter plates (Maxisorp, Nunc) were incubated with OVA solution in PBS (10 μg mL^{-1}, 100 μL) and incubated overnight at 4 °C. Subsequently, the plates were blocked with 4% milk (elk-milk, Campina, the Netherlands) and 0.1% Tween 20

in PBS solution (blocking buffer). Serial dilutions of the serum (100 μL) from each mouse were loaded on the OVA-coated plates. Then, 100 μL of goat anti-mouse total lgG-HRP conjugate (1 : 4000 dilution, Invitrogen) was added to each well after washing. The plates were incubated for 60 min at room temperature, washed with blocking buffer and subsequently incubated with 100 μL of 3,3′,5,5′-tetramethylbenzidine substrate solution (Sigma) in the dark for 10 min at room temperature. The enzyme reaction was stopped by adding 100 μL of 0.18 M H_2SO_4 to each well, and the absorbance was measured at 450 nm using SPECTROstar (BMG Labtech).

2.9 Statistical analysis

Graph Pad Prism software version 6 (GraphPad Software, Inc.) was used for statistical analysis. Comparison between groups was conducted with Student's *t* test. Differences in animal survival were calculated using the log-rank (ManteleCox) test. Statistical significance was considered when $p < 0.05$. Statistical analyses were done by comparison with the untreated group unless specified with markings.

3. Results and discussion

3.1 Preparation of OVA-loaded dextran particles and their interaction with DCs *in vitro*

Dextran-based cationic nanogels containing a pyridyldisulfide linker were prepared by inverse mini-emulsion photo-polymerization (as described in the Experimental section, Fig. 1).[33] When OVA, either native or derivatized with succinimidyl *S*-acetylthioacetate (SATA) groups, was incubated with a dispersion of the cationic nanogels in aqueous buffer of low ionic strength (HEPES, 20 mM, pH 7.4), the protein was almost quantitatively absorbed in these particles due to electrostatic interactions. Subsequently, SATA-derivatized OVA after deprotection of the SATA groups using hydroxyl amine was conjugated to the linker units in the nanogel *via* a thiol–disulfide exchange reaction. Non-reacted OVA was removed by washing with a high (physiological) ionic strength buffer (PBS, 167 mM, pH 7.4). Indeed, it was shown in our previous study that nanogels loaded with native OVA released the protein rapidly when the particles were dispersed in PBS. However, by conjugating OVA to the nanogels *via* disulfide bonds, the release of OVA in PBS only occurred in the presence of a reducing agent such as glutathione.[33] To obtain insight into the interaction between dextran gels and DCs, particles with various surface charge density (zeta potential) and size (around 0.2 and 2.5 micrometer diameter) were prepared (Table 1). While the microgels had a rather broad size distribution, the nanogels had a relatively low PDI.

It is known that DCs play a crucial role in activating the immune response because of their ability to take up and process antigens and subsequently present antigenic peptides to T cells.[9,13] In light of these DC functions, the capability of DCs to internalize Alexa 488 labeled dextran nanoparticles was visualized with confocal microscopy (Fig. 2A) and quantified using FACS (fluorescence-activated cell sorting, Fig. 2B). The binding and uptake studies were performed by incubation of labeled particles (and covalently loaded with modified OVA) with D1 dendritic cells for 24 h at 4 or 37 °C. Subsequently, the cells were treated with trypan blue (TB) to quench the Alexa 488-labeled particles that were surface associated with the cells (TB can quench green fluorescence and does not penetrate through cell membranes[39,46,47]). As shown in Fig. 2A, negligible binding and uptake were detected for (empty) neutral nanogels. On the other hand, positively charged nanogels and microgels, both loaded with conjugated OVA, showed strong association with the D1 cells. After incubation of D1 cells with TB, no significant decrease of fluorescence was found for nanogels with conjugated OVA, which indicates that they were internalized by D1 cells. However, both for nanogels of low charge and for microgels, the fluorescence signals on the cell surface was quenched by TB, which demonstrates that although these cationic particles were associated with the cells, they were not internalized as efficiently as the nanogels likely because of their lower charge and bigger size.[48–51] Interestingly, images of the cells incubated with the microgel formulation showed only small puncture spots inside the cells, suggesting that only a fraction of the smallest particles were taken up by the cells (keeping in mind the broad size distribution, Table 1), while the fluorescence of the larger particles was quenched outside the cells. Flow cytometry data (Fig. 2Ba) showed that the cationic nanoparticles were indeed associated with almost all cells whereas only ~5% of the cells showed binding of neutral nanogels. After quenching with TB, the percentage of positive cells

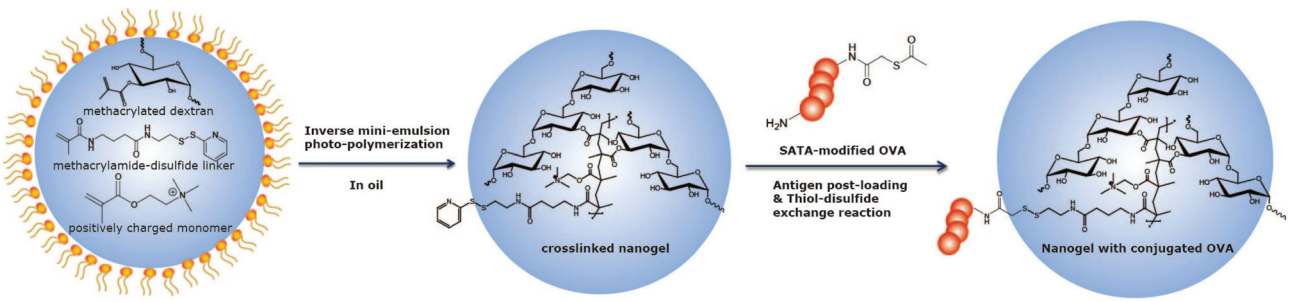

Fig. 1 Schematic representation of reduction-sensitive cationic dextran nanogels and conjugation of SATA-modified OVA.

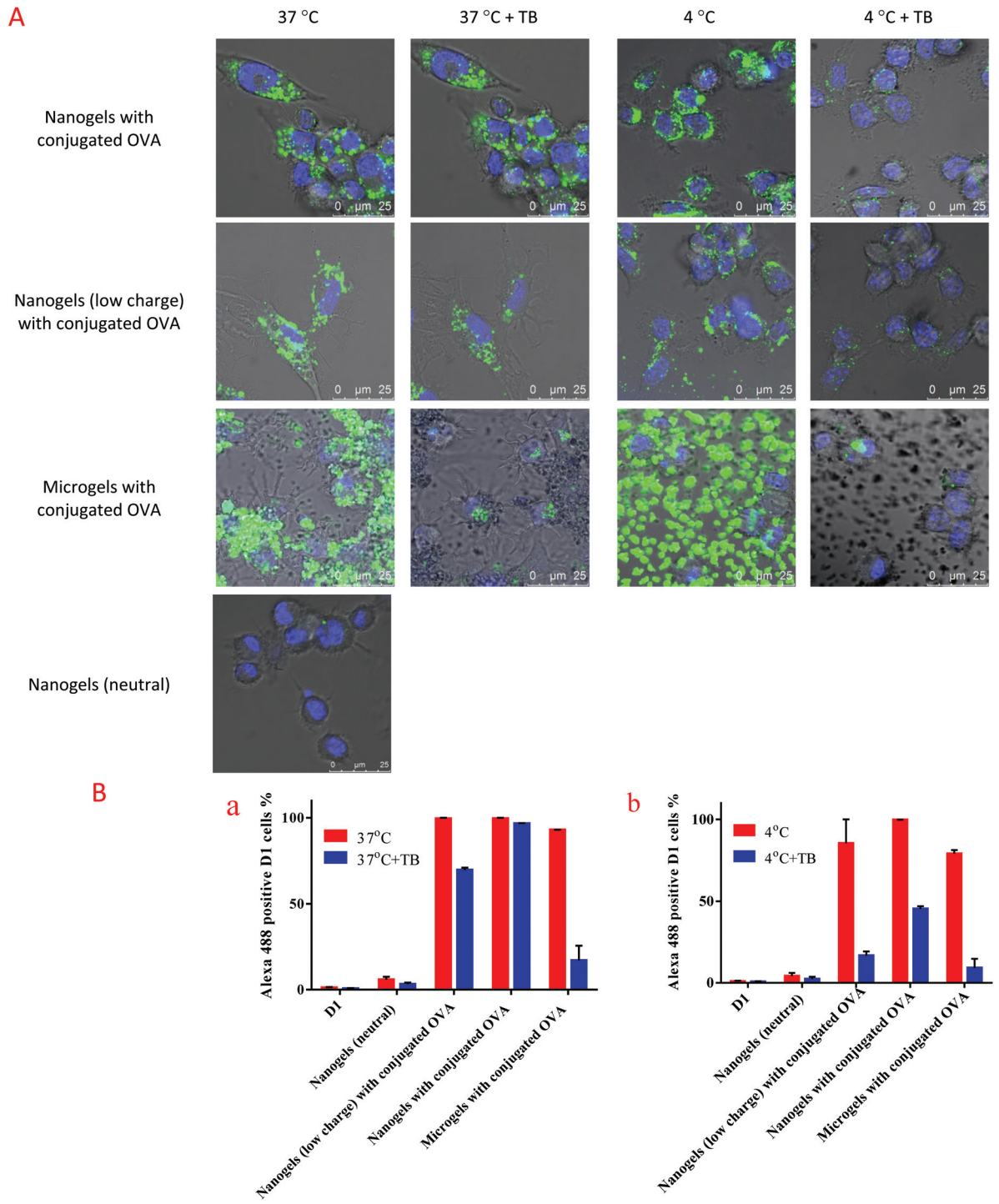

Fig. 2 Binding and internalization of Alexa 488 labeled particles (25 μg mL^{-1}) to DCs for 24 h at 4 or 37 °C before and after quenching with trypan blue (TB). (A) Confocal images of D1 cells after incubation with various Alexa 488 labeled particles. Nuclei were stained by Hoechst. (B) Binding and uptake of various Alexa 488 labeled particles to D1 cells quantified by flow cytometry at (a) 37 °C and (b) 4 °C.

previously incubated with nanogels with conjugated OVA did not change while these percentages dropped to 70% and 17% for cells incubated with low charged nanogels and microgels, respectively. These data are consistent with the confocal images shown in Fig. 2A. At 4 °C (Fig. 2A), binding on the surface of the cells was clearly seen for all cationic particles, but only limited signals were detected intracellularly after quenching with TB, demonstrating that at this temperature the particles are not internalized by DCs. The combined results of Fig. 2A and B demonstrate that the uptake of the

particles at 37 °C requires energy as previously shown for the uptake of different types of nanoparticles and nanomedicines by living cells.[51] Taken together, these results are in agreement with other reports showing that relatively highly cationic and small sized particles are efficiently taken up by DCs.[30,50–55] It should, however, be noted that the D1 cell line used for this uptake study is one subpopulation of DCs. The influence of particle size on cell uptake may be varied in other DC populations with different properties.

The capture and internalization of an antigen by DCs is the first step to trigger an immune response, while maturation of DCs is necessary to enhance T-cell response and prevent immune tolerance *in vivo*.[56–58] The maturation of DCs is characterized by upregulation of co-stimulatory molecules (such as CD40, CD80, and CD86) on their membrane and secretion of cytokines (such as IL-12, a T-cell growth and stimulating factor).[40,59,60] Cationic particles are able to maturate DCs although the exact mechanism is unknown at present.[30] To monitor DC maturation, D1 cells were incubated with, and stimulated by, different dextran nanoparticles for 24 h and subsequently analyzed for cell expression of activated markers (CD40 and CD86) and cytokine production (IL-12). All samples used in this study were tested by the limulus amebocyte lysate (LAL) assay, and the endotoxin content was below the detection level (0.1 EU mL^{-1}, ESI Table S1†). Poly(I:C) (1 μg mL^{-1}), a known immunostimulant of DCs,[61,62] was used as a positive control. The flow cytometry data presented in Fig. 3(Aa and Ab) show that D1 cells incubated with cationic particles upregulated expression of both CD40 and CD86 and the percentage of matured DCs increased with the surface charge of the

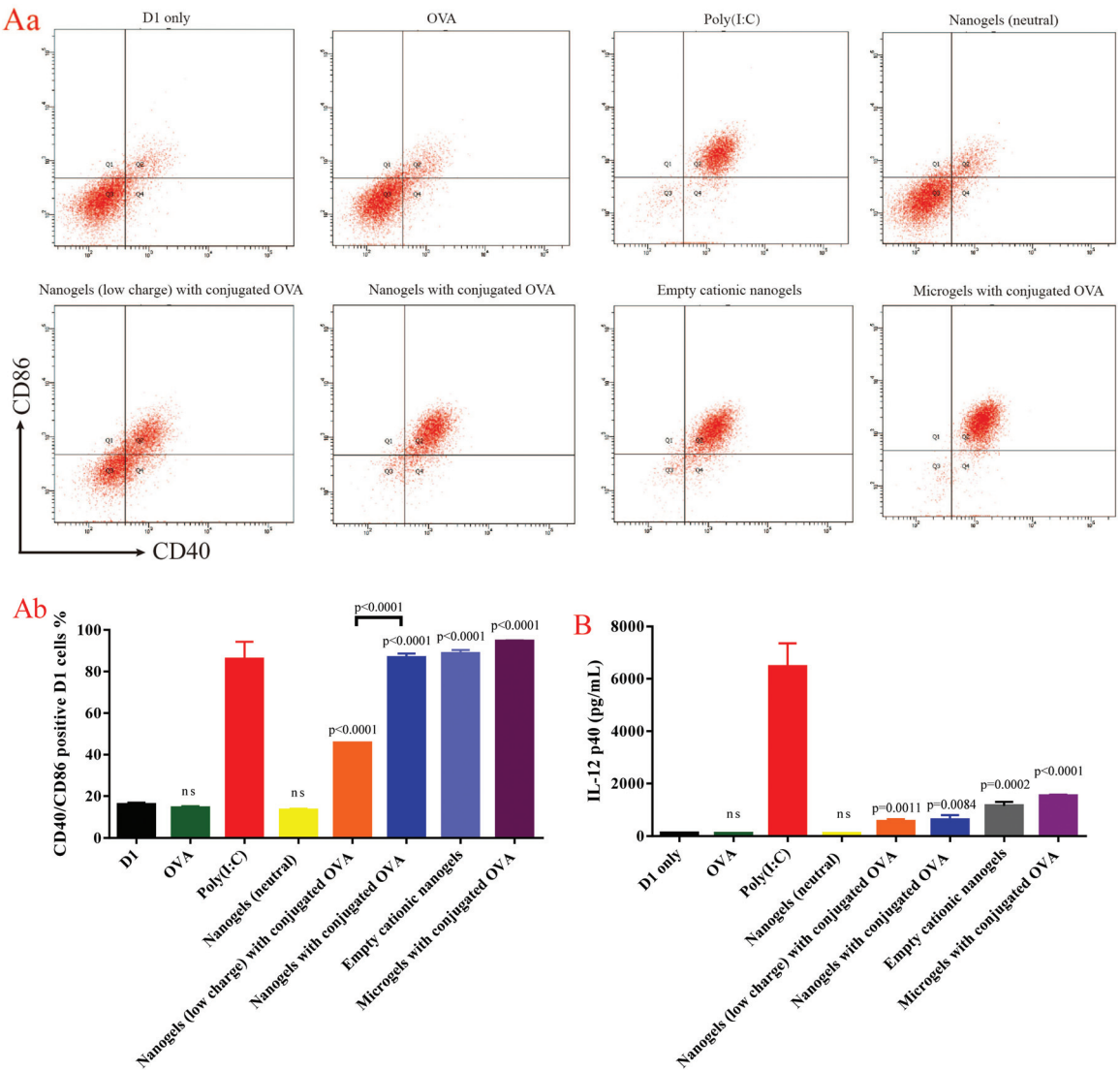

Fig. 3 Flow cytometry analysis of DC maturation and cytokine secretion upon incubation with dextran particles. (Aa, Ab) Quantification of CD40 and CD86 expression after 24 h incubation with various particles. (B) Secretion of IL-12. Poly(I:C) was used as positive control. Statistical analyses were done by comparison with the untreated group (D1 only). ns, not significant.

particles. Meanwhile, soluble OVA and neutral nanogels did not upregulate the expression of these markers on DCs. Taken together, the maturation of DCs is due to the charge of the particles. Moreover, relatively highly cationic particles demonstrated increased IL-12 secretion when compared to neutral/low charge nanogels, though not as efficiently as poly(I:C) (Fig. 3B).

Further studies were focused on the localization of the best performing nanogels (*i.e.* with conjugated OVA) in DCs and the subsequent processing of OVA from these nanogels. Nanogels with conjugated OVA and labeled with Alexa 488 were incubated with D1 cells for 2, 5 and 24 h before confocal images were taken, and lysotracker-red was used to label lysosomes. Already after 2 h, most of the nanogels were bound or taken up by D1 cells and the internalized nanogels colocalized with lysotracker (Fig. 4A, yellow spots). Signals from the nanogels inside the cells still overlapped with the lysotracker at 5 and 24 h, which indicates that internalized nanogel particles remained in the lysosomes. To investigate the processing of the antigen by DCs, DQ-OVA was conjugated in the nanogels and subsequently incubated with D1 cells. DQ-OVA is heavily labeled with BODIPY (boron-dipyrromethene) dyes, which leads to strong fluorescence quenching.[63] Once DQ-OVA is processed by DCs into single, dye-labeled peptides, the quenching

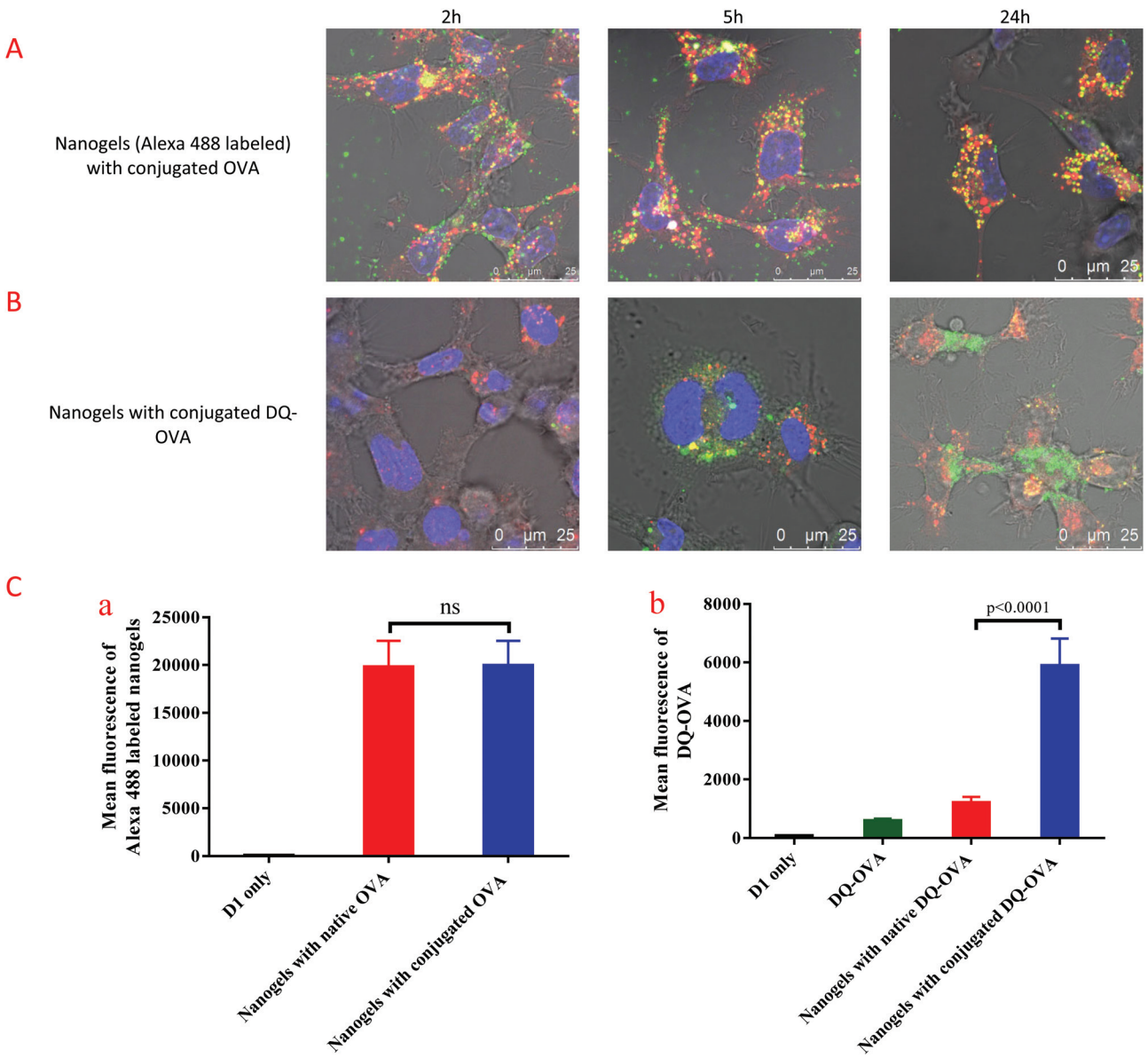

Fig. 4 *In vitro* uptake and processing of OVA loaded nanogels by D1 cells. Confocal images of D1 cells incubated with, respectively, (A) Alexa 488 labeled nanogels (green) and (B) nanogels with conjugated DQ-OVA (green) for 2, 5 and 24 h. Lysosomes (red) were labeled by incubation with lysotracker-red 1 h before taking images and nuclei were stained by Hoechst in blue. (C) (a) Nanogel uptake and (b) DQ-OVA processing after 24 h incubation with D1 cells measured by flow cytometry. ns, not significant.

is relieved, resulting in bright fluorescence signals. Fig. 4B shows that hardly any green fluorescence signal from DQ-OVA was observed after 2 h. However, fluorescence signals of this label were detected but not colocalized with lysotracker-red after 5 h and the signals became stronger after 24 h. These signals were homogenously distributed, which demonstrated that DQ-OVA was digested by D1 cells into small peptides which localized in the cytosol. Taken together, these images indicate that although the nanogels were trapped in the endo/lysosomes, the released and processed antigen was transported to the cytosol, which is crucial for MHC class I antigen presentation to activate a T cell response.[4,12,13,26] It is also revealed (Fig. 4Ca) that nanogels were equally taken up regardless of whether OVA was conjugated or just physically loaded. However, the processed fragments of DQ-OVA were dramatically enhanced by nearly 5-fold when modified DQ-OVA was conjugated to nanogels *via* disulfide bonds compared to when native DQ-OVA was encapsulated but not conjugated (Fig. 4Cb). This indicates that a higher amount of OVA was delivered intracellularly to DCs by conjugation to the reduction-sensitive linkers.

The results presented above suggest that OVA is efficiently delivered into DCs by reduction-sensitive nanogels and that OVA or antigenic peptides can be transported to the cytosol of DCs. Moreover, cationic nanogels have the ability to stimulate and maturate DCs. From the above we selected nanogels with conjugated OVA for *in vivo* studies and used nanogels with native OVA as a control.

3.2 Preventive antitumor effect of nanogels with conjugated OVA by prophylactic vaccination

To investigate the protective efficacy of the nanogels with conjugated OVA against cancer, we tested formulations (for details of the particulate formulations see ESI Table S2†) in a prophylactic vaccination setting using the B16-OVA melanoma model (expressing OVA antigen).[45] It has been shown that the specific T cell immune response induced by the tumor antigen recognizes the antigenic peptide determinants presented by the MHC molecules of the tumor and attacks and kills tumor cells. In this study, mice were immunized with nanogels with conjugated OVA and 7 control groups were used to prove the feasibility of the intracellular delivery of the antigen. C57BL/6 mice (10 per group) received various formulations subcutaneously (s.c.) on day 0 and 14 as a prime and boost, and the mice were challenged with an injection of 1.5×10^5 B16-OVA cells s.c. at day 28 post boost (Fig. 5A). OVA specific $CD8^+$ T cells and antibodies were measured 7 days after the prime and boost, and the volume of the developing tumor was monitored over time after the challenge.

Fig. 5B shows that for the negative control mice (PBS and empty nanogels group), the inoculation of B16-OVA cells resulted in palpable tumors (~2 × 2 mm) in most mice from day 6, followed by rapid tumor development. Within 20 days, all mice in these negative control groups were euthanized due to a tumor size >2000 mm^3 (Fig. 5C). In contrast, mice immunized with free or formulated OVA demonstrated tumor inhibition and overall increased survival efficacy in the prophylactic model. Nanogels with native OVA (*i.e.* non-conjugated), as expected, showed immune capacity similar to that of soluble OVA because the loading of the native OVA was based only on electrostatic interactions causing a rapid release from nanogels in medium with physiological ionic strength.[33] In the groups receiving these soluble OVA and nanogels with the native OVA, all mice developed a tumor but the growth was slower and the survival increased compared to the negative controls indicating some effect of the free OVA in this model. We observed further reduction in tumor growth and longer survival duration in the mice when the soluble OVA and nanogels with the native OVA were combined with poly(I:C). Fig. 5C shows that the percentages of tumor-free mice at day 52 were 20% (two out of ten mice) for the soluble OVA + poly(I:C) group and 30% for nanogels with the native OVA + poly(I:C). This result is in agreement with previous publications in which it was shown that poly(I:C) containing vaccines reduced tumor growth in animals because the immunological danger signals given by this adjuvant enhanced vaccine-induced antitumor immune responses.[41,44,61,62] Interestingly, the tumor growth kinetics in the group that received nanogels with conjugated OVA but without poly(I:C) partly overlapped with those that received the soluble OVA or nanogels with native OVA supplemented with poly(I:C), and four out of ten mice were tumor free until the end of study (80 days). This indicates that coupling of the antigen to the nanogel network *via* reducible bonds induces prophylactic tumor immunity similar to those of formulations containing free OVA plus the strong adjuvant poly(I:C). Apparently, a higher amount of antigen was delivered and released into the DCs by the nanogel with a conjugated OVA formulation, which is sufficient to induce effective immunity against this specific antigen. Most importantly, the formulation of nanogels with conjugated OVA + poly(I:C) was the most effective, since only one out of ten mice developed a tumor and this tumor started growing at a significantly later time point (~day 20) as compared to the other groups (day 6). Likely, intracellular delivery of the antigen into DCs in combination with activation of these cells by poly(I:C) leads to an effective cellular immune response which can control lethal tumor growth.

To assess the capacity of the various OVA formulations to raise specific $CD8^+$ T cell levels, blood samples of the mice 7 days after the prime and boost vaccination were analyzed *ex vivo*. OVA specific $CD8^+$ T cells were identified with flow cytometry after tetramer staining using APC-conjugated SIINFEKL/H2-Kb tetramers and PE-conjugated anti-mouse CD8a mAb.[44,45] The gating strategy for analysis of the percentage of H-2Kb-SIINFEKL tetramer $CD8^+$ T cells is described in the ESI Fig. S2.† Fig. 5D shows that prime vaccination with soluble OVA and nanogels with native OVA did not result in more antigen specific T cells than observed for the control groups. On the other hand, soluble OVA and nanogels with native OVA formulated with poly(I:C) did enhance cellular response, and the number of antigen specific $CD8^+$ T cells detected in the blood was significantly higher than those in

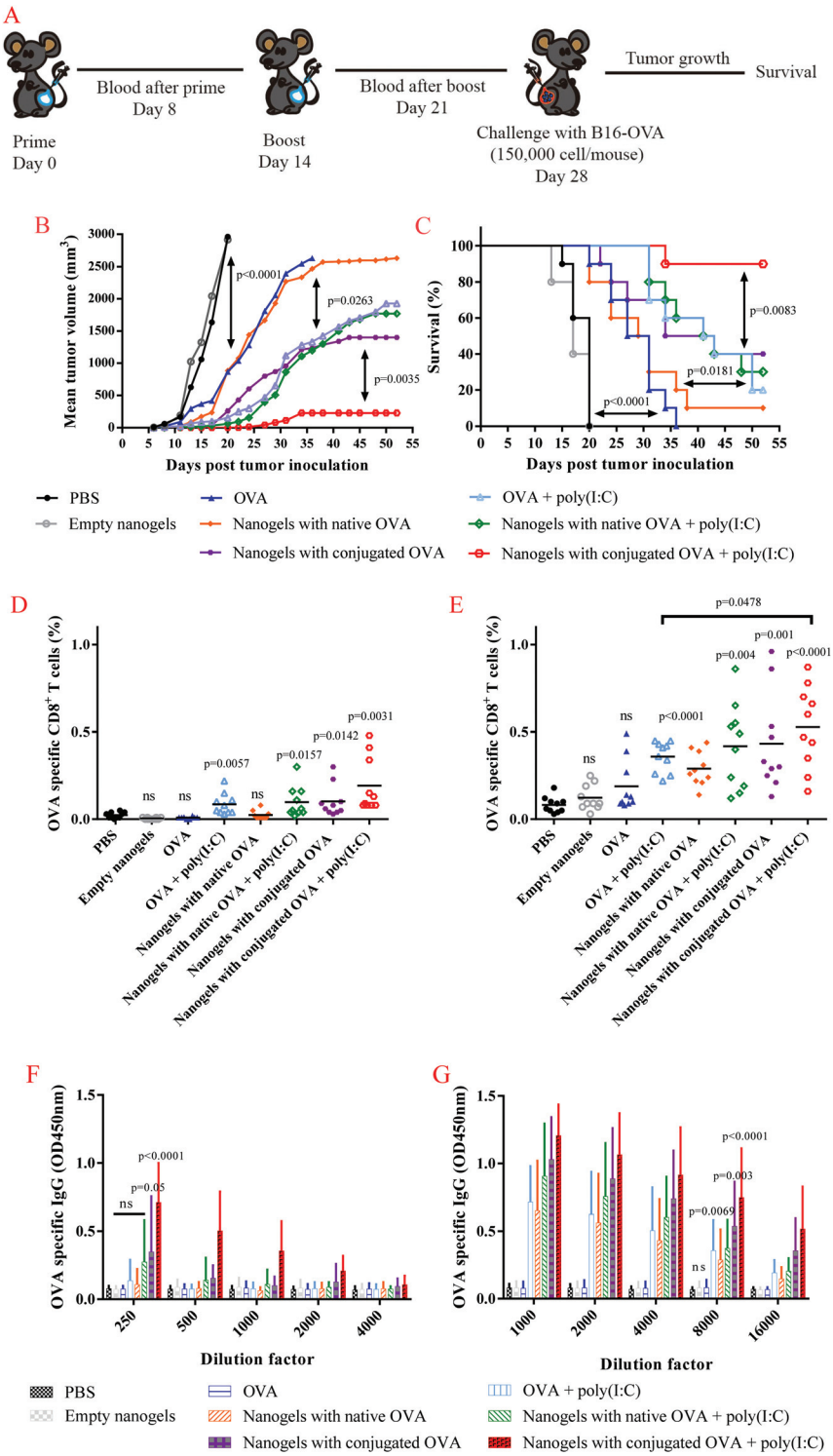

Fig. 5 (A) Prophylactic vaccination scheme for OVA loaded nanogel formulations as prophylactic tumor vaccines in mice. Female C57BL/6 mice (n = 10 per group) were immunized with various formulations (50 μg OVA (and 20 μg poly(I:C)) per mouse) according to the scheme A. (B) Tumor growth shown as mean (n = 10) over 52 days post tumor challenge. SEM (standard error of the mean) are shown in the ESI, Fig. S1A.† When one mouse was sacrificed, its end-point tumor size remained included in the calculations of the mean sizes after sacrificing. (C) Survival of mice (n = 10). One week after (D) prime and (E) boost, blood samples were analyzed for OVA specific $CD8^+$ T cells by tetramer staining using FACS. OVA specific total IgG was measured in the serum of diluted blood samples collected after (F) prime and (G) boost. Statistical analyses were done by comparison with the untreated group unless specified with markings. ns, not significant.

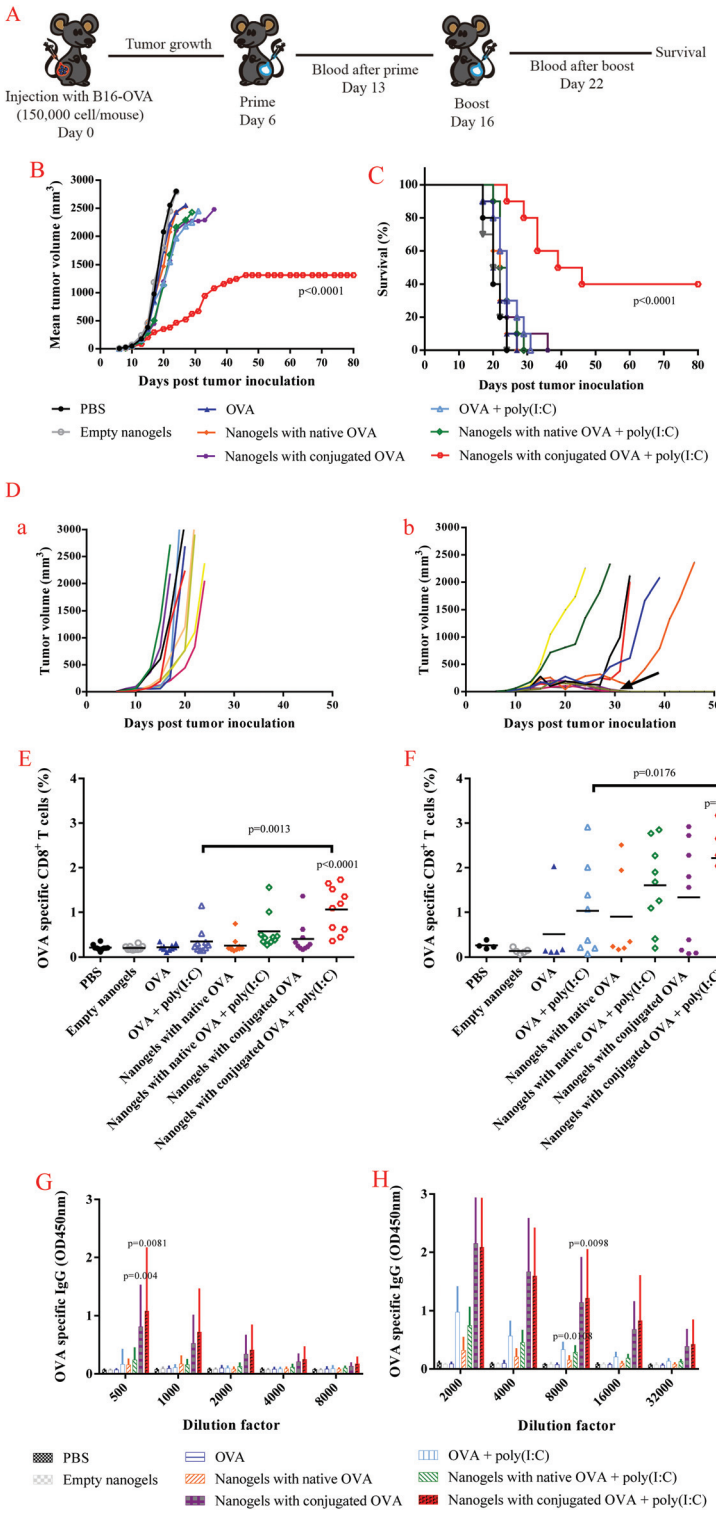

Fig. 6 (A) Therapeutic vaccination for OVA-loaded nanogels in a tumor model. (B) Tumor growth in an established B16-OVA tumor model following treatment with various vaccine formulations. The mean tumor size was calculated from 10 mice in each group, SEM (standard error of the mean) are shown in ESI Fig. S1B.† When one mouse was sacrificed, its end-point tumor size remained included in the calculations of the mean sizes after sacrificing. (C) Survival following treatment. (D) Tumor growth of each individual mouse treated with (a) PBS and (b) nanogels with conjugated OVA + poly(I:C). The black arrow (Db) points out the curves of four mice in the base line which are tumor-free. Expansion of OVA specific $CD8^+$ T cells in the blood (E) 7 days after prime and (F) 6 days after boost. Anti-OVA IgG concentrations in sera after (G) prime and (H) boost. Different numbers of mice in each group were sacrificed before the second blood sampling and the data are collected from the remaining mice. Statistical analyses were done by comparison with the untreated group. ns, not significant.

the non-adjuvanted group. Vaccination with nanogels with conjugated OVA gave the same level of OVA specific $CD8^+$ T cells as the soluble OVA nanogels with native OVA supplemented with poly(I:C), which is in line with the above presented antitumor effect. The mice that were immunized with nanogels with conjugated OVA + poly(I:C) had the highest average number of OVA specific $CD8^+$ T cells. As shown in Fig. 5E, the boost vaccinations also led to the highest level of OVA specific $CD8^+$ T cells. Overall, the conjugated OVA enhanced vaccine-induced CTLs responses more effectively than the other formulations did. The antitumor immunity observed in the different groups correlated with the levels of OVA specific $CD8^+$ T cells.

Whole protein is capable of inducing both $CD8^+$ and $CD4^+$ antigen-specific responses because it contains multiple epitopes which can be present in both MHC class I and II pathways.[64] Since the whole protein was used as the antigen, we also evaluated the effect of the conjugates on the induction of a humoral immune response. OVA specific IgG antibodies were measured in the serum of the mice one week after the prime and boost. In Fig. 5F and G, the serum anti-OVA IgG titers are shown for mice that received the same dose of OVA delivered with various formulations, and for the negative controls. No antibodies were detected in the blood of mice immunized with free OVA and negative controls. Nanogels with native OVA induced the production of IgG at notably low levels, while other formulations elicited higher levels of anti-OVA IgG with a similar trend as for the specific $CD8^+$ T cells; nanogels with conjugated OVA + poly(I:C) induced the highest levels of antibodies. The concentrations of OVA specific IgG measured in serum after the boost substantially increased except in the serum of mice that received the negative controls and soluble OVA. Moreover, even though nanogels with native OVA produced remarkable higher antibody titers than soluble OVA after the boost, the tumors of the mice in these two groups showed similar growth after the challenge. This indicates that antigen specific antibodies are not the determining factor for antitumor immunity. This is in agreement with publications in which it is shown that T cells are considered to be the major immune cells involved in tumor clearance, and therefore an effective strategy for cancer immunotherapy is to activate specific T cells that recognize tumors.[12,44,56,65]

3.3 Tumor growth inhibition of established melanoma by nanogels with conjugated OVA therapeutic vaccination

The therapeutic potential of nanogels with conjugated OVA was evaluated according to the vaccination scheme shown in Fig. 6A. B16-OVA cells were injected at day 0 and palpable tumors (~2 × 2 mm) were detected approximately 6 days post injection. Mice were then vaccinated with various formulations by giving prime and boost s.c. injections at day 6 and 16, respectively. As soon as palpable tumors appeared, tumor volumes increased rapidly in the mice of the control groups (injected with PBS or empty nanogels) (Fig. 6B). This figure also shows that no beneficial effect on tumor growth was found for mice receiving soluble OVA and nanogels with native OVA as compared to those of the control groups. Soluble OVA + poly(I:C), nanogels with native OVA + poly(I:C) and nanogels with conjugated OVA slightly retarded the growth of the tumors when compared with the control groups. Importantly, we observed that following tumor onset, the mean tumor size of mice vaccinated with nanogels with conjugated OVA + poly(I:C) remained relatively small and it took a relatively long time for tumors to grow, so that the overall survival of this group (>80 days) was significantly better compared with all other groups (36 days when all mice were sacrificed). Although the mean tumor size increased continuously, the tumor growth was not the same for each mouse in the nanogels with conjugated OVA + poly(I:C) group (Fig. 6D). Two mice out of ten displayed rapid tumor growth despite the treatment, while four mice showed a significant delay in tumor growth (*i.e.* the tumors started growing rapidly just after day 29). Strikingly, four mice showed complete elimination of these aggressive tumors and remained tumor free until the end of the 80-day study showing the potency of this vaccine formulation.

To analyze the antigen specific response raised by the vaccines in mice carrying established tumors, antigen specific $CD8^+$ T cells (Fig. 6E and F) and antigen specific antibodies (Fig. 6G and H) in blood were measured one week after the prime and boost, respectively. In agreement with observations on the prophylactic experiment, soluble OVA and nanogels with native OVA raised similar levels of T cells and antibodies as observed for the negative control groups after the prime and boost. Soluble OVA + poly(I:C) and nanogels with native OVA + poly(I:C) vaccines induced stronger proliferation of antigen specific $CD8^+$ T cells and resulted in higher OVA specific antibodies, while nanogels with conjugated OVA + poly(I:C) showed substantially higher activation and proliferation of T cells and antibody production. Interestingly, antigen specific T cells and IgG reached significantly higher levels (~4 times) than those detected in the prophylactic model after the prime. This is in agreement with those reported in literature,[29,66,67] and it is likely because the immune response was already activated by the presence of antigen-expressing tumor cells in these mice and reactivated by the vaccines. It should be noted that B16-OVA is an aggressive cell line and efficient treatment at early stage is needed.[42,65,68] Among all 8 groups, only mice immunized with nanogels with conjugated OVA + poly(I:C) showed reduction of tumors, likely because the antigen specific T cell levels in these mice were significantly higher than those in the other groups, which is sufficient to inhibit tumor growth already after the first vaccination.

4. Conclusions

This study demonstrates that cationic dextran nanogels are efficiently internalized by DCs, and able to maturate DCs *in vitro*. They facilitated disulfide-linked OVA delivery to DCs, and their subsequent processing and transportation to the cytosol of the cells. Furthermore, these OVA-nanogel conjugates increased antigen specific T cell levels and antibody

production, and thus induced a strong protective and curative effect against melanoma *in vivo*. 4/10 mice showed complete regression of the aggressive melanoma tumor and remained tumor free for a period of at least 80 days. Collectively, the investigations presented in this paper demonstrate that intracellular delivery of antigens by these novel nanogels is a promising strategy to induce effective antigen specific immunity against cancer.

Acknowledgements

The research was partially supported by China Scholarship Council.

Notes and references

1 J. Couzin-Frankel, *Science*, 2013, **342**, 1432–1433.
2 K. K. Wong, W. A. Li, D. J. Mooney and G. Dranoff, in *Advances in Immunology*, ed. D. S. Robert, Academic Press, 2016, vol. 130, pp. 191–249.
3 N. K. Mehta, K. D. Moynihan and D. J. Irvine, *Cancer Immunol. Res.*, 2015, **3**, 836–843.
4 J. M. Vyas, A. G. Van der Veen and H. L. Ploegh, *Nat. Rev. Immunol.*, 2008, **8**, 607–618.
5 A. Dani, A. Chaudhry, P. Mukherjee, D. Rajagopal, S. Bhatia, A. George, V. Bal, S. Rath and S. Mayor, *J. Cell Sci.*, 2004, **117**, 4219–4230.
6 J. P. Griffin, R. Chu and C. V. Harding, *J. Immunol.*, 1997, **158**, 1523–1532.
7 P. A. Roche and K. Furuta, *Nat. Rev. Immunol.*, 2015, **15**, 203–216.
8 C. G. Drake, E. J. Lipson and J. R. Brahmer, *Nat. Rev. Clin Oncol.*, 2014, **11**, 24–37.
9 K. Palucka and J. Banchereau, *Immunity*, 2013, **39**, 38–48.
10 J. J. Glass, D. Yuen, J. Rae, A. P. Johnston, R. G. Parton, S. J. Kent and R. De Rose, *Nanoscale*, 2016, **8**, 8255–8265.
11 K. K. Phua, S. K. Nair and K. W. Leong, *Nanoscale*, 2014, **6**, 7715–7729.
12 O. P. Joffre, E. Segura, A. Savina and S. Amigorena, *Nat. Rev. Immunol.*, 2012, **12**, 557–569.
13 S. Nierkens, J. Tel, E. Janssen and G. J. Adema, *Trends Immunol.*, 2013, **34**, 361–370.
14 H. Yue, W. Wei, Z. Gu, D. Ni, N. Luo, Z. Yang, L. Zhao, J. A. Garate, R. Zhou, Z. Su and G. Ma, *Nanoscale*, 2015, **7**, 19949–19957.
15 S. Rahimian, M. F. Fransen, J. W. Kleinovink, J. R. Christensen, M. Amidi, W. E. Hennink and F. Ossendorp, *J. Controlled Release*, 2015, **203**, 16–22.
16 K. K. Ahmed, S. M. Geary and A. K. Salem, *J. Pharm. Sci.*, 2016, **105**, 1173–1179.
17 S. M. Geary, Q. Hu, V. B. Joshi, N. B. Bowden and A. K. Salem, *J. Controlled Release*, 2015, **220**(Part B), 682–690.
18 H. Li, K. Fierens, Z. Zhang, N. Vanparijs, M. J. Schuijs, K. Van Steendam, N. Feiner Gracia, R. De Rycke, T. De Beer, A. De Beuckelaer, S. De Koker, D. Deforce, L. Albertazzi, J. Grooten, B. N. Lambrecht and B. G. De Geest, *ACS Appl. Mater. Interfaces*, 2016, **8**, 1147–1155.
19 S. De Koker, K. Fierens, M. Dierendonck, R. De Rycke, B. N. Lambrecht, J. Grooten, J. P. Remon and B. G. De Geest, *J. Controlled Release*, 2014, **195**, 99–109.
20 L. Gu and D. J. Mooney, *Nat. Rev. Cancer*, 2016, **16**, 56–66.
21 A. S. Cheung, S. T. Koshy, A. G. Stafford, M. M. C. Bastings and D. J. Mooney, *Small*, 2016, **12**, 2321–2333.
22 D. J. Irvine, M. C. Hanson, K. Rakhra and T. Tokatlian, *Chem. Rev.*, 2015, **115**, 11109–11146.
23 K. T. Mody, A. Popat, D. Mahony, A. S. Cavallaro, C. Yu and N. Mitter, *Nanoscale*, 2013, **5**, 5167–5179.
24 Y. Tao, Y. Zhang, E. Ju, H. Ren and J. Ren, *Nanoscale*, 2015, **7**, 12419–12426.
25 G. Zhu, Y. Liu, X. Yang, Y. H. Kim, H. Zhang, R. Jia, H. S. Liao, A. Jin, J. Lin, M. Aronova, R. Leapman, Z. Nie, G. Niu and X. Chen, *Nanoscale*, 2016, **8**, 6684–6692.
26 N. M. Molino, A. K. L. Anderson, E. L. Nelson and S.-W. Wang, *ACS Nano*, 2013, **7**, 9743–9752.
27 M. S. Goldberg, *Cell*, 2015, **161**, 201–204.
28 L. Xu, J. Xiang, Y. Liu, J. Xu, Y. Luo, L. Feng, Z. Liu and R. Peng, *Nanoscale*, 2016, **8**, 3785–3795.
29 M. Håkerud, P. K. Selbo, Y. Waeckerle-Men, E. Contassot, P. Dziunycz, T. M. Kündig, A. Høgset and P. Johansen, *J. Controlled Release*, 2015, **198**, 10–17.
30 Y. Ma, Y. Zhuang, X. Xie, C. Wang, F. Wang, D. Zhou, J. Zeng and L. Cai, *Nanoscale*, 2011, **3**, 2307–2314.
31 M. C. Hanson, M. P. Crespo, W. Abraham, K. D. Moynihan, G. L. Szeto, S. H. Chen, M. B. Melo, S. Mueller and D. J. Irvine, *J. Clin. Invest.*, 2015, **125**, 2532–2546.
32 H. Gong, J. Xiang, L. Xu, X. Song, Z. Dong, R. Peng and Z. Liu, *Nanoscale*, 2015, **7**, 19282–19292.
33 D. Li, N. Kordalivand, M. F. Fransen, F. Ossendorp, K. Raemdonck, T. Vermonden, W. E. Hennink and C. F. van Nostrum, *Adv. Funct. Mater.*, 2015, **25**, 2993–3003.
34 W. N. E. van Dijk-Wolthuis, O. Franssen, H. Talsma, M. J. van Steenbergen, J. J. Kettenes-van den Bosch and W. E. Hennink, *Macromolecules*, 1995, **28**, 6317–6322.
35 E. Verheyen, L. Delain-Bioton, S. van der Wal, N. el Morabit, A. Barendregt, W. E. Hennink and C. F. van Nostrum, *Macromol. Biosci.*, 2010, **10**, 1517–1526.
36 C. Winzler, P. Rovere, M. Rescigno, F. Granucci, G. Penna, L. Adorini, V. S. Zimmermann, J. Davoust and P. Ricciardi-Castagnoli, *J. Exp. Med.*, 1997, **185**, 317–328.
37 B. A. Pulaski, K. Y. Yeh, N. Shastri, K. M. Maltby, D. P. Penney, E. M. Lord and J. G. Frelinger, *Proc. Natl. Acad. Sci. U. S. A.*, 1996, **93**, 3669–3674.
38 B. Naeye, K. Raemdonck, K. Remaut, B. Sproat, J. Demeester and S. C. De Smedt, *Eur. J. Pharm. Sci.*, 2010, **40**, 342–351.
39 G. K. Srivastava, R. Reinoso, A. K. Singh, I. Fernandez-Bueno, D. Hileeto, M. Martino, M. T. Garcia-Gutierrez, J. M. Pigazo Merino, N. F. Alonso, A. Corell and J. C. Pastor, *Exp. Eye Res.*, 2011, **93**, 956–962.

40 C. Hsieh, S. Macatonia, C. Tripp, S. Wolf, A. O'Garra and K. Murphy, *Science*, 1993, **260**, 547–549.
41 F. Aranda, D. Llopiz, N. Díaz-Valdés, J. I. Riezu-Boj, J. Bezunartea, M. Ruiz, M. Martínez, M. Durantez, C. Mansilla, J. Prieto, J. J. Lasarte, F. Borrás-Cuesta and P. Sarobe, *Cancer Res.*, 2011, **71**, 3214–3224.
42 K. K. Phua, H. F. Staats, K. W. Leong and S. K. Nair, *Sci. Rep.*, 2014, **4**, 5128.
43 C. Yang, X. Ren, D. Ding, L. Wang and Z. Yang, *Nanoscale*, 2016, **8**, 10768–10773.
44 R. A. Rosalia, L. J. Cruz, S. van Duikeren, A. T. Tromp, A. L. Silva, W. Jiskoot, T. de Gruijl, C. Löwik, J. Oostendorp, S. H. van der Burg and F. Ossendorp, *Biomaterials*, 2015, **40**, 88–97.
45 S. Mandl, L. J. Sigal, K. L. Rock and R. Andino, *Proc. Natl. Acad. Sci. U. S. A.*, 1998, **95**, 8216–8221.
46 J. Nuutila and E.-M. Lilius, *Cytometry, Part A*, 2005, **65A**, 93–102.
47 D. Mahony, A. S. Cavallaro, K. T. Mody, L. Xiong, T. J. Mahony, S. Z. Qiao and N. Mitter, *Nanoscale*, 2014, **6**, 6617–6626.
48 F. Shima, T. Uto, T. Akagi, M. Baba and M. Akashi, *Acta Biomater.*, 2013, **9**, 8894–8901.
49 L.-C. Cheng, X. Jiang, J. Wang, C. Chen and R.-S. Liu, *Nanoscale*, 2013, **5**, 3547–3569.
50 F. Blank, P. A. Stumbles, E. Seydoux, P. G. Holt, A. Fink, B. Rothen-Rutishauser, D. H. Strickland and C. von Garnier, *Am. J. Respir. Cell Mol. Biol.*, 2013, **49**, 67–77.
51 H. Jin, D. A. Heller, R. Sharma and M. S. Strano, *ACS Nano*, 2009, **3**, 149–158.
52 S. D. Xiang, A. Scholzen, G. Minigo, C. David, V. Apostolopoulos, P. L. Mottram and M. Plebanski, *Methods*, 2006, **40**, 1–9.
53 V. B. Joshi, S. M. Geary and A. K. Salem, *AAPS J.*, 2013, **15**, 85–94.
54 N. Benne, J. van Duijn, J. Kuiper, W. Jiskoot and B. Slütter, *J. Controlled Release*, 2016, **234**, 124–134.
55 C. Foged, B. Brodin, S. Frokjaer and A. Sundblad, *Int. J. Pharm.*, 2005, **298**, 315–322.
56 S. Sakaguchi, T. Yamaguchi, T. Nomura and M. Ono, *Cell*, 2008, **133**, 775–787.
57 S. Fallarini, T. Paoletti, C. O. Battaglini, P. Ronchi, L. Lay, R. Bonomi, S. Jha, F. Mancin, P. Scrimin and G. Lombardi, *Nanoscale*, 2013, **5**, 390–400.
58 S. L. Haughney, K. A. Ross, P. M. Boggiatto, M. J. Wannemuehler and B. Narasimhan, *Nanoscale*, 2014, **6**, 13770–13778.
59 A. Slawek, T. Maj and A. Chelmonska-Soyta, *Am. J. Reprod. Immunol.*, 2013, **70**, 116–126.
60 S. W. Van Gool, P. Vandenberghe, M. d. Boer and J. L. Ceuppens, *Immunol. Rev.*, 1996, **153**, 47–83.
61 R. Ammi, J. De Waele, Y. Willemen, I. Van Brussel, D. M. Schrijvers, E. Lion and E. L. J. Smits, *Pharmacol. Ther.*, 2015, **146**, 120–131.
62 A. M. Hafner, B. Corthésy and H. P. Merkle, *Adv. Drug Delivery Rev.*, 2013, **65**, 1386–1399.
63 L. J. Young, N. S. Wilson, P. Schnorrer, A. Mount, R. J. Lundie, N. L. La Gruta, B. S. Crabb, G. T. Belz, W. R. Heath and J. A. Villadangos, *Proc. Natl. Acad. Sci. U. S. A.*, 2007, **104**, 17753–17758.
64 D. S. Pouniotis, S. Esparon, V. Apostolopoulos and G. A. Pietersz, *Immunol. Cell Biol.*, 2011, **89**, 904–913.
65 M. Merad, T. Sugie, E. G. Engleman and L. Fong, *Blood*, 2002, **99**, 1676–1682.
66 S. Neumann, K. Young, B. Compton, R. Anderson, G. Painter and S. Hook, *Vaccine*, 2015, **33**, 5838–5844.
67 D. H. Schuurhuis, N. van Montfoort, A. Ioan-Facsinay, R. Jiawan, M. Camps, J. Nouta, C. J. Melief, J. S. Verbeek and F. Ossendorp, *J. Immunol.*, 2006, **176**, 4573–4580.
68 T. Kottke, N. Boisgerault, R. M. Diaz, O. Donnelly, D. Rommelfanger-Konkol, J. Pulido, J. Thompson, D. Mukhopadhyay, R. Kaspar, M. Coffey, H. Pandha, A. Melcher, K. Harrington, P. Selby and R. Vile, *Nat. Med.*, 2013, **19**, 1625–1631.